

NUSTAR DETECTION OF QUIESCENT HARD X-RAY EMISSION FROM SGR 0526–66 IN THE LARGE MAGELLANIC CLOUD

SANGWOOK PARK^{1,4}, JAYANT BHALERAO¹, OLEG KARGALTSEV², AND PATRICK O. SLANE³

Accepted by The Astrophysical Journal

ABSTRACT

The soft γ -ray repeater (SGR) 0526–66 is the first-identified magnetar, and is projected within the supernova remnant N49 in the Large Magellanic Cloud. Based on our ~ 50 ks *NuSTAR* observation, we detect the quiescent-state 0526–66 for the first time in the 10–40 keV band. Based on the joint analysis of our *NuSTAR* and the archival *Chandra* ACIS data, we firmly establish the presence of the nonthermal component in the X-ray spectrum of 0526–66 in addition to the thermal emission. In the best-fit blackbody (BB) plus power law (PL) model, the slope of the PL component (photon index $\Gamma = 2.1$) is steeper than those ($\Gamma \lesssim 1.5$) for other magnetars. The soft part of the X-ray spectrum can be described with a BB component with the temperature of $kT = 0.43$ keV. The best-fit radius ($R = 6.5$ km) of the X-ray-emitting area is smaller than the canonical size of a neutron star. If we assume an underlying cool BB component with the canonical radius of $R = 10$ km for the neutron star in addition to the hot BB component (2BB + PL model), a lower BB temperature of $kT = 0.24$ keV is obtained for the passively cooling neutron star’s surface, while the hot spot emission with $kT = 0.46$ keV dominates the thermal spectrum ($\sim 85\%$ of the thermal luminosity in the 0.5–5 keV band). The nonthermal component ($\Gamma \sim 1.8$) is still required.

Subject headings: X-rays: individual (SGR 0526–66) — stars: neutron — X-rays: stars

1. INTRODUCTION

The soft γ -ray repeater (SGR) 0526–66 showed intense γ -ray outbursts on 1979 March 5 and a luminous pulsed afterglow with $P \sim 8$ s (Mazets et al. 1979; Cline et al. 1980), which led to the discovery of the magnetar phenomenon. The quiescent soft X-ray counterpart is projected within the supernova remnant (SNR) N49 in the Large Magellanic Cloud (LMC) (Rothschild et al. 1994), and its pulsations with $P = 8.0436$ s and $\dot{P} = 6.6 \times 10^{-11}$ s s⁻¹ were detected with a low pulsed-fraction of $f_p \sim 10\%$ in the *Chandra* data (Kulkarni et al. 2003). Later *Chandra* and *XMM-Newton* data showed that the spin-down rate (\dot{P}) might have decreased by $\sim 40\%$ over the course of several years (Tiengo et al. 2009; Güver et al. 2012). The estimated pulsed-fraction appeared to decrease to $f_p \sim 4\%$ by 2009 (Güver et al. 2012). Evidence of a slow decay ($\sim 20\text{--}30\%$ in ~ 17 yr until 2009) in the soft X-ray flux was reported, which may be related to its long-term surface cooling and/or evolution of the X-ray emitting hot spot areas (Park et al. 2012; Güver et al. 2012).

The 1 – 10 keV band *XMM-Newton* spectrum can be fitted with a simple power law (PL) model with a steep photon index ($\Gamma \sim 3.3$) (Tiengo et al. 2009). The 0.5 – 6 keV band *Chandra* spectrum (based on simultaneous spectral model fits of six data sets taken in 2000, 2001, and 2009 with $\sim 30\text{--}50$ ks individual exposures) was fitted with spectral models for the X-ray emission from a magnetized H-atmosphere ($kT \sim 0.35$ keV) of a neu-

tron star (Güver et al. 2012). The *Chandra* data with higher photon count statistics (with ~ 110 ks effective exposure in total, combining four observations taken in 2009) showed that two-component models, e.g., thermal blackbody (BB) and/or nonthermal PL components, are required to adequately fit the observed X-ray spectrum in the 0.4 – 8 keV band (Park et al. 2012). In the two-component spectral model fits, the soft component of the observed X-ray spectrum might be attributed to emission from the surface cooling neutron star (a BB-like emission with $kT \sim 0.4$ keV). Depending on the adopted spectral models, a hot spot(s) (e.g., BB with $kT \sim 1$ keV and $R \sim 1$ km) or the nonthermal magnetospheric radiation (e.g., a PL with $\Gamma \sim 2.5$) were required to fit the remaining part of the X-ray spectrum, primarily in the $\sim 3\text{--}8$ keV band.

Broadband X-ray spectroscopy covering $E > 10$ keV is crucial to establish the properties of the nonthermal component and to discriminate between the hotter thermal and nonthermal emission. Here we report the results from our ~ 50 ks *NuSTAR* observation, which provides the detection of the hard X-ray emission from 0526–66 up to $E \sim 40$ keV. We also present results from our joint analysis of the broadband X-ray spectrum (in the 0.4 – 40 keV band) of 0526–66 based on our *NuSTAR* and the archival *Chandra* data. We describe the observations and the data reduction in Section 2. We present our data analysis in Sections 3 & 4, and a discussion in Section 5. A summary is presented in Section 6.

2. OBSERVATIONS & DATA

We observed 0526–66 with *NuSTAR* on 2018 February 7 during Cycle 3. We processed the data with NuSTAR-DAS (NuSTAR Data Analysis Software) version 1.7.1 and *NuSTAR* CALDB version 20180126. After the standard data reduction, the effective exposure is 47 ks. We

¹ Box 19059, Department of Physics, University of Texas at Arlington, Arlington, TX 76019

² Department of Physics, George Washington University, 725 21st Street NW, Washington, DC 20052

³ Harvard-Smithsonian Center for Astrophysics, 60 Garden Street, Cambridge, MA 02138

⁴ s.park@uta.edu

extracted the *NuSTAR* spectrum of 0526–66 from a circular source region with a radius of $30''$, centered on the source position RA (J2000) = $05^h 26^m 01^s.61$, and Dec (J2000) = $-66^\circ 04' 46''.0$. We extracted the background spectrum from an annular region around the source. The source and background spectra and spectral response files were created with the standard HEASARC software NPIPELINE tool. Combining the data taken with two Focal Plane Modules (FPMA and FPMB), we extracted ~ 1200 counts from the source extraction region in the 2 – 40 keV band. We estimate that $\sim 25\%$ of them are due to the background, while the remaining (~ 900 counts) comprises both the SGR and emission from SNR N49 (Figure 1 and Section 3). Based on our spectral model fits (see Section 3), we estimate the total background including the contamination by N49 is $\sim 60\%$ of the total extracted counts in the 2 – 40 keV band. In the 10 – 40 keV band, we extract ~ 280 counts, $\sim 50\%$ of which is the background. The contamination from SNR N49 is negligible in this band. Thus, we make a clear $\sim 8\sigma$ (~ 140 background-subtracted counts) detection of 0526–66 in the 10 – 40 keV band.

About 1/4 of the field of view in the north-northeast of the source was moderately affected by scattered X-rays from nearby bright X-ray sources (Figure 1). The low-mass X-ray binary LMC X-3, which is projected at ~ 2.4 northeast of 0526–66, is the only bright X-ray source within a few degrees in the north-northeast of 0526–66. Thus, although LMC X-3 was not in a high state during our *NuSTAR* observation of 0526–66 (based on the archival MAXI data), the contaminating source appears to be LMC X-3. 0526–66 is positioned close to (or just outside of) the boundary of the affected background region (Figure 1). Based on our background spectral extractions from several regions around the source, we estimated a $\sim 10\%$ contamination from these scattered X-rays on the 10 – 40 keV band source flux, which would not significantly affect our analysis. In the following sections we assume the average background spectrum, extracted from an annular region around the source (Figure 1).

As supplementary data to model the broadband X-ray spectrum of 0526–66, we jointly analyzed the archival *Chandra* data of 0526–66 taken with the Advanced CCD Imaging Spectrometer (ACIS) in 2009 (ObsIDs 10123, 10806, 10807, and 10808)⁵. A 1/4 subarray of the ACIS-S3 detector was used in these archival *Chandra* data, which ensured a low photon pileup ($< 5\%$) for a reliable spectral analysis of 0526–66. We processed each of the raw data sets and merged them, following the standard data reduction methods as described in Park et al. (2012). We extracted the source spectrum from a circular region centered on the source position ($2''$ in radius). Since 0526–66 is projected within the boundary of

the X-ray emitting shell of SNR N49, the background characterization based on the high resolution imaging spectroscopy with *Chandra* ACIS data is critical. We extracted the background spectrum from an annular region around the source within SNR N49. Based on these data we extract ~ 21000 photons (including $\sim 12\%$ background) for 0526–66 in the 0.4–8 keV band.

3. X-RAY SPECTRAL ANALYSIS

The main goal of the *NuSTAR* observation of 0526–66 is to search for hard X-ray emission at $E \gtrsim 10$ keV. While we make a clear detection of 0526–66 in the 10 – 40 keV band, the utility of the *NuSTAR* data alone to adequately characterize the soft X-ray spectrum of 0526–66 is limited, because of the poor count statistics in the soft X-ray band (i.e., no response at $E < 2$ keV for FPM and the significant contamination from SNR N49’s thermal emission at $E < 5$ keV). Thus, we perform the *NuSTAR* + *Chandra* joint spectral analysis to fit the broadband X-ray spectrum of 0526–66. For our spectral analysis we rebinned both of *NuSTAR* and *Chandra* spectra to contain a minimum of 20 counts per energy channel, and perform all spectral model fits in the 0.4 – 40 keV band. In our spectral model fits, we fixed the Galactic column at $N_{\text{H,Gal}} = 6 \times 10^{20} \text{ cm}^{-2}$ toward 0526–66 (Dickey & Lockman 1990). We fit the foreground column in the LMC ($N_{\text{H,LMC}}$) assuming the LMC abundances available in the literature (He = 0.89, C = 0.30, N = 0.12, O = 0.26, Ne = 0.33, Na = 0.30, Mg = 0.32, Al = 0.30, Si = 0.30, S = 0.31, Cl = 0.31, Ar = 0.54, Ca = 0.34, Cr = 0.61, Fe = 0.36, Co = 0.30, and Ni = 0.62, Russell & Dopita 1992; Hughes et al. 1998). Hereafter, elemental abundances are with respect to solar (Anders & Grevesse 1989). We tested recent X-ray measurements of the LMC abundances for O, Ne, Mg, and Fe, which were based on the X-ray spectral model fits of the shocked interstellar medium in the LMC SNRs (Maggi et al. 2016; Schenck et al. 2016) for our $N_{\text{H,LMC}}$ parameter. These LMC abundance measurements are lower than the previous values by $\sim 30\text{--}50\%$, which resulted in slight increases (by $\sim 10\text{--}20\%$) for the best-fit $N_{\text{H,LMC}}$. Otherwise, the impact of these LMC abundances on the results from our spectral model fits of 0526–66 is not statistically significant, and thus does not affect our conclusions. For self-consistent comparisons with the previous results in the literature, we assumed the LMC abundances listed above in this work.

In our spectral model fits, we tied $N_{\text{H,LMC}}$, the BB temperature, the BB-emitting area, the PL photon index and normalization (see Sections 3.1 & 3.2 for our adopted spectral models) between the *NuSTAR* and *Chandra* spectra. At $E \lesssim 7$ keV, the contamination from the soft thermal X-ray emission from SNR N49 (whose angular extent is $\sim 1'$, Figure 1) is substantial in the *NuSTAR* spectrum of 0526–66 due to the large PSF ($58''$ HPD, Harrison et al. 2013) of *NuSTAR*. To account for this SNR spectrum, we added a plane-shock (PS) component (with the electron temperature of the hot gas $kT \sim 1$ keV on average, based on Park et al. [2003] and Uchida et al. [2015]) in the spectral modeling of the *NuSTAR* spectrum of 0526–66. We find that this background emission component from SNR N49 contributes $\sim 40\%$ of the *NuSTAR* flux of 0526–66 in the 2 – 7 keV band, and is negligible ($< 5\%$ of the total flux) in the 7

⁵ This is a “single” observation, which was split into four sub-sequences over a relatively short two-month period to accommodate the restrictions on the solar pitch angles for the telescope. There are several other *Chandra* archival data sets of 0526–66, which were taken several years earlier with shorter exposures than these 2009 data. Taking advantage of the longest effective exposure and the closest epoch of the observation (to that of our *NuSTAR* observation), we use these 2009 *Chandra* data for the joint spectral analysis in this work. The large PSF of *XMM-Newton* resulted in a significant contamination from SNR N49 in the soft X-ray band spectrum of 0526–66 (Tiengo et al. 2009). Thus, we do not use the archival *XMM-Newton* data in this work.

– 40 keV band. Thanks to the sub-arcsecond resolution of the *Chandra* ACIS data, the contamination from the SNR in the *Chandra* spectrum of 0526–66 is small. We subtracted it from the total spectrum of the source (Section 2), rather than applying this additional PS model component for the *Chandra* spectrum.

3.1. Thermal Spectral Models for Hard Component

There are several publicly-available spectral models for the X-ray spectrum emitted by the neutron star’s hot atmosphere with various atomic compositions, such as the NSA model (Pavlov et al. 1995) and NSMAX models (Ho et al. 2008; Mori & Ho 2007). While these atmospheric models are more physically-motivated to describe the observed X-ray spectra from neutron stars, they are not adequate for magnetars, whose magnetic fields are very strong: e.g., these models allow the magnetic fields up to $B \sim 10^{13}$ G, whereas $B \sim 10^{14-15}$ has been estimated for 0526–66. Thus, we chose to use simple BB models for the thermal component of the X-ray spectrum of 0526–66 in this work, realizing that they may provide only a phenomenological (rather than physically accurate) description of the data. We note that fits with the BB model still allow us to investigate the thermal vs. nonthermal nature of the X-ray spectrum, and would also enable self-consistent comparisons with the results from the magnetar analysis in the literature (where the BB models are commonly adopted).

In agreement with the previously published spectral analysis of the same *Chandra* observations (Park et al. 2012), we find that the single BB model cannot fit the observed broadband X-ray spectrum of 0526–66 ($\chi^2/\nu \sim 3$). Then, we applied two component spectral models. To test the thermal origin of the hard component of its X-ray spectrum, we fitted the broadband X-ray spectrum of 0526–66 with a two-component BB model. In this spectral model fit, we initially fixed the cool and hot component BB temperatures at the values derived by Park et al. (2012): i.e., $kT_{soft} \approx 0.4$ keV and $kT_{hard} \approx 1$ keV. The best-fit model is statistically poor ($\chi^2/\nu \sim 1.5$) because our *NuSTAR* spectrum at $E \gtrsim 7$ keV cannot be fitted with the BB model. When it is fitted, the temperature of the hot BB component increases to $kT \approx 2$ keV for the improved best-fit ($\chi^2/\nu \sim 1.3$). However, the systematic excess in the *NuSTAR* spectrum is still evident at $E \gtrsim 10$ keV ($\chi^2/\nu = 2.7$ in the 10 – 40 keV band), even with this high temperature (Figure 2a). Thus, we conclude that the two-temperature BB model cannot adequately describe the *NuSTAR* + *Chandra* spectrum of 0526–66.

3.2. Nonthermal Spectral Models for Hard Component

We first attempted a single PL model fit to the broadband X-ray spectrum of 0526–66. The best-fit PL model is statistically unacceptable ($\chi^2/\nu = 1.8$), showing significant residuals both in the soft ($E < 2$ keV) and the hard bands ($E > 5$ keV). Next, we fitted the broadband X-ray spectrum of 0526 with BB + PL models. The best-fit model results in $kT_{BB} = 0.43$ keV and the PL photon index $\Gamma = 2.10$ ($\chi^2/\nu = 1.09$, Figures 2b & 3). This best-fit BB + PL model indicates an emission radius of the neutron star $R_{NS} \approx 6.5$ km. These results are summarized in Table 1.

Recent *NuSTAR* observations of magnetars and anomalous X-ray pulsars have shown the presence of similar hard X-ray emission components at $E > 10$ keV, for which the broadband X-ray spectrum was fitted with three-component (2BB + PL) spectral models (e.g., Gotthelf et al. 2019). Taking a similar approach, we apply 2BB + PL model fits for 0526–66. In these model fits, we assume the canonical radius of neutron stars ($R_{NS} = 10$ km) for the emitting area of the soft component BB spectrum. The best-fit model ($\chi^2/\nu = 1.09$) implies $kT_{TH1} = 0.24$ keV for the cooling surface of the neutron star. The best-fit hot spot temperature is $kT_{TH2} = 0.46$ keV with $R \approx 6$ km for the emitting area. In this model fit, a slightly harder PL component with the best-fit $\Gamma = 1.84$ is obtained. Although the statistical improvement in the spectral fit with the 2BB + PL model is marginal (the F-probability ~ 0.02), the consideration of a cooler emission component from the neutron star with the canonical size may be useful to understand the physical nature of 0526–66, and thus we include the results from this 2BB + PL model fit in Table 1.

4. NUSTAR TIMING ANALYSIS

Due to poor photon statistics and the large background (~ 500 counts per FPM in the 2 – 40 keV band with $\sim 60\%$ background [including the contamination from N49]), the pulsation search (for the presumed small $f_p \lesssim 10\%$) is difficult with our *NuSTAR* data. Based on the previously reported values of \dot{P} and P , we calculated Z_1^2 statistic as a function of frequency within a plausible range of $P = 8.044 - 8.076$ s (Güver et al. 2012) using events from both FPMA and FPMB with the arrival times corrected for the Earth and spacecraft motion. We did not find any statistically significant signal with the two largest values of $Z_{1,max}^2 \approx 10$ (both are found near 8.05348 s). Therefore, we calculate an upper limit on the pulsed fraction (for a sinusoidal pulse profile with a single peak per period) as $f_{p,n\sigma}^{obs} \approx 2 [\ln(\mathcal{N}/P_n)/N]^{1/2}$ where, $N = 1159$ is the total number of events (source plus background), $\mathcal{N} = 183$ is the number of independent frequency trials, and $P_n = \text{erfc}(n/\sqrt{2}) \approx (2/\pi)^{1/2} e^{-n^2/2}/n$ (for $n > 2$) with n being the confidence level in units of standard deviation σ . For $n = 3$, $P_n \approx 0.003$ and, hence, $f_{p,3\sigma}^{obs} = 0.195$ is an upper limit on the observed pulsed fraction at 3σ confidence. The corresponding intrinsic pulsed fraction is $f_{p,3\sigma}^{int} = f_{p,3\sigma}^{obs} (N/N_{bg}) = 0.48$ because the background is contributing 60% of the total events within the source extraction aperture, $r = 30''$, in the 2 – 40 keV band.

5. DISCUSSION

5.1. Broadband X-Ray Spectral Nature of 0526–66

Based on our *NuSTAR* and *Chandra* data analysis, we find that a PL-like nonthermal spectral component, in addition to the soft thermal BB component, is required to adequately fit the broadband X-ray spectrum of 0526–66. In our BB + PL model fits, a BB temperature of $kT \approx 0.43$ keV is estimated, where the implied radius of the emission region ($R \approx 6.5$ km at the distance of $d = 50$ kpc) is smaller than the canonical neutron star size ($R \sim 10$ km). The best-fit 2BB + PL model shows a lower BB temperature of $kT = 0.24$

keV, assuming the neutron star radius of $R_{\text{NS}} = 10$ km. The cooler ($kT = 0.24$ keV) component BB flux contributes $\sim 15\%$ of the total BB luminosity in the 0.5 – 5 keV band. Thus, for both of the BB + PL and 2BB + PL model fits, the BB component with $kT \sim 0.4 - 0.5$ keV dominates the thermal component X-ray emission of 0526–66. Spin-down ages of $\tau_{sd} \sim 2000 - 3400$ yr have been estimated for 0526–66 (Kulkarni et al. 2003; Tiengo et al. 2009; Güver et al. 2012). While the physical association between SGR 0526–66 and SNR N49 is in debate (see Section 5.2), these spin-down ages are in plausible agreement (within a factor of ~ 2) with the estimated Sedov age of SNR N49 ($\tau_{\text{Sedov}} \sim 4800$ yr, Park et al. 2012). Thus, we may estimate the age of 0526–66 to be $\tau \sim 10^{3-4}$ yr. If either of these BB temperatures corresponds to that of the passively cooling neutron star’s surface after its birth, 0526–66 is hotter than the predictions of the cooling curves for neutron stars of this age (Yakovlev & Pethick 2004). For a neutron star in this age range, the estimated high surface temperature may suggest a re-heating of the surface, probably due to the recent burst activity, and/or strong magnetic field effects on the thermal evolution of the neutron star (Pons et al. 2009; Viganó et al. 2013).

Based on our best-fit spectral models, we estimate that the hardness ratio for the unabsorbed X-ray flux ($\text{HR} = f_{15-60 \text{ keV}}/f_{1-10 \text{ keV}}$ as utilized by Enoto et al. [2017]) is $\text{HR} \sim 0.3-0.4$ (depending on the adopted model). The latest estimates for the time-derivative of the pulsation period, the magnetic field strength, and the characteristic age for 0526–66 are $\dot{P} \sim 4 \times 10^{-11}$ s s^{-1} , $B \sim 4 \times 10^{14}$ G, and $\tau_{sd} \sim 3200$ yr, respectively (Güver et al. 2012). We compare our estimated HR values for 0526–66 with the PL-like empirical relations with \dot{P} , B , and the neutron star’s age, which were suggested based on the Galactic sample of a \sim dozen magnetars (Enoto et al. 2017). Our estimated range of HR for 0526–66 is lower than $\text{HR} \sim 1$ that is predicted by Enoto et al. (2017). \dot{P} (and thus B) for 0526–66 appears to be decreasing between 2000 and 2009 (Kulkarni et al. 2003; Tiengo et al. 2009; Güver et al. 2012). The soft X-ray flux of 0526–66 has been decaying between 1992 and 2009 (Park et al. 2012; Güver et al. 2012). It is difficult to estimate changes in the BB temperature of 0526–66 between 2009 and 2018. The *NuSTAR*’s detector response is limited to $E > 2$ keV, and the soft X-ray spectrum (at $E \lesssim 5$ keV) of 0526–66 in the *NuSTAR* data is significantly contaminated by that from SNR N49. Based on the BB + PL model fit to our *NuSTAR* data alone with an assumption that the BB emitting area stays the same as it was in 2009, we place a 2σ upper limit of $kT_{\text{BB}} \lesssim 0.5$ keV for the thermal component emission of 0526–66 as of 2018. Considering the possible temporal evolution in \dot{P} , B , and kT , we speculate that it might be partially responsible for the low HR. Our estimated limits on kT_{BB} and f_p as of 2018 based on our *NuSTAR* data are not constraining due to poor photon statistics. Significantly deeper *NuSTAR* and *Chandra* observations would be required to constrain the recent evolution of these critical neutron star parameters.

Our spectral fits indicate the photon index $\Gamma \sim 2$ for the PL component which dominates the hard X-ray spectrum of 0526–66 at $E \gtrsim 10$ keV. This spectral slope of the

PL component is larger than those measured for other Galactic magnetars ($\Gamma \lesssim 1.5$, e.g., Enoto et al. [2017]). Apparently, 0526–66 has not shown any activity since its giant bursts in 1979, being in the quiescent state (probably with a steady cooling) for the longest time period among the observed magnetars. We speculate that this distinctive evolutionary state of 0526–66 (compared with that for other magnetars with more frequent burst activity) in the last several decades might have led to a steeper nonthermal spectral component, and thus somewhat lower HR in the latest broadband X-ray spectrum. The best-fit PL photon index for 0526–66 is similar to that of the synchrotron emission spectrum from the relativistically accelerated electrons in pulsar magnetospheres, or from pulsar wind nebulae (PWNe, although some PWNe show harder spectra with $\Gamma \sim 1.0 - 1.5$). However, the high-resolution *Chandra* ACIS images show no evidence for an extended nebulosity around the pointlike source 0526–66 (Kulkarni et al. 2003; Park et al. 2012). If we entertained the intriguing possibility of a PWN being developed for 0526–66, the lack of an observed extended nebula in the *Chandra* data would require an angular size of $\lesssim 1''$ that cannot be resolved by *Chandra*. The corresponding physical size is $\lesssim 0.2$ pc at the distance of the LMC ($d = 50$ kpc), which would be similar to (or smaller than) those of the torus and jet associated with young pulsars found in the Galactic SNRs G292.0+1.8 (Park et al. 2007) and 3C58 (Slane et al. 2002).

5.2. Notes on Foreground Absorption for 0526–66

SGR 0526–66 is projected within the boundary of SNR N49 in the LMC (Cline et al. 1982; Rothschild et al. 1994). However, the physical association between the two has not been conclusive. The statistical chance probability for a coincidental alignment along the line of sight between N49 and 0526–66 is not negligible (Gaensler et al. 2001). If the massive progenitor of 0526–66 was born in a nearby massive stellar cluster, a significantly older age ($\sim 10^5$ yr) than that of N49 (~ 4800 yr) is implied for 0526–66 (Klose et al. 2004). In our spectral model fits, the contribution from the PL component is considerable in the soft band X-ray flux (at $E < 2$ keV) as well as in the hard band ($E > 5$ keV). This results in an inferred foreground LMC column $N_{\text{H,LMC}} \sim 3 \times 10^{21}$ cm^{-2} toward 0526–66 (Table 1), a factor of ~ 2 larger than that estimated for SNR N49. This higher LMC column for 0526–66 might cast further doubt on its physical association with N49. When we fixed the LMC column at the value estimated for N49 ($N_{\text{H,LMC}} \sim 1.5 \times 10^{21}$ cm^{-2} , Park et al. 2012), the overall spectral model fits (for those models presented in Table 1) became slightly poorer ($\chi^2/\nu \sim 1.14$). Although these fits may be formally distinguished from those summarized in Table 1 (e.g., F -probability ~ 6 and 1×10^{-4} , for the BB + PL and 2BB + PL model fits, respectively), the overall fits may still be considered to be statistically acceptable. Also, due to the model-dependence of these $N_{\text{H,LMC}}$ estimates (between 0526–66 and N49) and the relatively large uncertainties, it may not be straightforward to firmly conclude that the X-ray spectrum of 0526–66 is more absorbed than that of N49.

We have confidently detected SGR 0526–66 in the quiescent state at $E > 10$ keV with *NuSTAR*. The joint spectral fits to the *NuSTAR* + *Chandra* spectrum require at least two component model if BB and PL are used for the individual components. The hard X-ray emission at $E > 10$ keV, which is fitted with a PL spectrum, is most likely nonthermal in origin. The slope of the PL component ($\Gamma \sim 1.8 - 2.1$) is softer than those for other magnetars observed with *NuSTAR*. For our best-fit BB + PL model, we obtain a high BB temperature of $kT \approx 0.43$ keV, and the estimated radius of the X-ray-emitting area ($R \approx 6.5$ km) is smaller than the canonical size of a neutron star. If we assumed the BB spectrum from the cooling neutron star with a standard radius of $R_{\text{NS}} = 10$ km in addition to the hot $kT \sim 0.4$ keV component, a lower BB temperature of $kT \approx 0.24$ keV is obtained for the passively cooling surface of the neutron star. The presence of the

relatively soft PL component in the X-ray spectrum of 0526–66 may provide an intriguing opportunity to study the magneto-thermal evolution of a magnetar during the substantially long quiescent period of several decades after the strong outbursts. Based on the *NuSTAR* data, we place a 3σ upper limit of $f_p \sim 0.48$ on the intrinsic pulsed fraction of 0526–66 in the 2 – 40 keV band.

We thank the anonymous referee for her/his comments that helped improving this manuscript. This work has been supported in part by NASA *NuSTAR* grant 80NSSC17K0633 and the *Chandra* grant GO9-0072A to the University of Texas at Arlington. O. K. was supported in part by NASA through *Chandra* Award number TM8-19005B issued by the *Chandra* X-Ray Center which is operated by the Smithsonian Astrophysical Observatory for and on behalf of NASA under the contract NAS8-03060.

REFERENCES

- Anders, E., & Grevesse, N. 1989, *Geochimica et Cosmochimica Acta*, 53, 197
- Cline, T. L., Desai, U. D., Pizzichini, G., Teegarden, B. J., Evans, W. D., Klebesadel, R. W., Laros, J. G., Hurley, K., Niel, M., & Vedrenne, G. 1980, *ApJ*, 237, L1
- Cline, T. L., Desai, U. D., Teegarden, B. J., Evans, W. D., Klebesadel, R. W., Laros, J. G., Barat, C., Hurley, K., et al. 1982, *ApJ*, 255, L45
- Dickey, J. M., & Lockman, F. J. 1990, *ARA&A*, 28, 215
- Enoto, T. et al. 2017, *ApJS*, 231, 8
- Gaensler, B. M., Slane, P. O., Gotthelf, E. V., & Vasisht, G. 2001, *ApJ*, 559, 963
- Gotthelf, E. V. et al. 2019, *ApJ*, 874, 25
- Güver, T., Göğüş, E., & Özel, F. 2012, *MNRAS*, 424, 210
- Ho, W. C. G., Potekhin, A. Y., & Chabrier, G., 2008, *ApJS*, 178, 102
- Hughes, J. P., Hayashi, I., & Koyama, K. 1998, *ApJ*, 505, 732
- Klose, S. et al. 2004, *ApJ*, 609, L13
- Kulkarni, S. R., Kaplan, D. L., Marshall, H. L., Frail, D. A., Murakami, T., & Yonetoku, D. 2003, *ApJ*, 585, 948
- Maggi, P., Haberl, F., Kavanagh, P. J., Sasaki, M., Bozzetto, L. M., Filipović, M. D., Vasilopoulos, G., Pietsch, W., Points, S. D., Chu, Y. -H., Dickel, J., Ehle, M., Williams, R., & Greiner, J. 2016, *A&A*, 585A, 162
- Mazets, E. P., Golentskii, S. V., Ilinskii, V. N., Aptekar, R. L., & Guryan, Iu. A. 1979, *Nature*, 282, 587
- Mori, K. & No, W. C. G. 2007, *MNRAS*, 377, 905
- Park, S., Burrows, D. N., Garmire, G. P., Nousek, J. A., Hughes, J. P., & Williams, R. M. 2003, *ApJ*, 586, 210
- Park, S., Hughes, J. P., Slane, P. O., Burrows, D. N., Gaensler, B. M., & Ghavamian, P. 2007, *ApJ*, 670, L121
- Park, S., Hughes, J. P., Slane, P. O., Burrows, D. N., Lee, J.-J., & Mori, K. 2012, *ApJ*, 748, 117
- Pavlov, G.G., Shibano, Y. A. Zvliv, V. E., & Meyer, R. D. 1995, in “The Lives of the Neutron Stars,” ed. M.A. Alpar, U. Kiziloglu, & J. van Paradijs (NATO ASI Ser. C, 450; Dordrecht: Kluwer), p. 71
- Pons, J. A., Miralles, J. A., & Geppert, U. 2009, *A&A*, 496, 207
- Rothschild, R. E., Kulkarni, S. R., & Lingefelter, R.E. 1994, *Nature*, 368, 432
- Russell, S. C., & Dopita, M. A., 1992, *ApJ*, 384, 508
- Schenck, A., Park, S., & Post, S. 2016, *AJ*, 151, 161
- Slane, P. O., Helfand, D. J., & Murray, S. S. 2002, *ApJ*, 571, L45
- Tiengo, A., Esposito, P., Mereghetti, S., Israel, G. L., Stella, L., Turolla, R., Zane, S., Rea, N., Götz, D., & Feroci, M. 2009, *MNRAS*, 399L, L74
- Uchida, H., Koyama, K., & Yamaguchi, H. 2015, *ApJ*, 808, 77
- Viganó, D., Rea, N., Pons, J. A., Perna, R., Aguilera, D. N., & Miralles, J. A., 2013, *MNRAS*, 434, 123
- Yakovlev, D. G., & Pethick, C. J., 2004, *ARA&A*, 42, 169

TABLE 1
SUMMARY OF SPECTRAL MODEL FITS TO SGR 0526–66

Model Parameter	BB + PL	2BB + PL
kT_{TH1} (keV)	0.43 ± 0.01	$0.24^{+0.05}_{-0.06}$
kT_{TH2} (keV)	-	$0.46^{+0.05}_{-0.03}$
Γ	$2.10^{+0.16}_{-0.22}$	1.84 ± 0.24
R_{TH1} (km)	6.5 ± 0.5	10 (fixed)
R_{TH2} (km)	-	$5.9^{+0.8}_{-1.3}$
f_{TH}^{a} (0.5 – 5 keV, 10^{-13} erg cm^{-2} s^{-1})	$4.5^{+0.5}_{-0.8}$	$5.7^{+0.7}_{-1.2}$
f_{PL}^{a} (5 – 40 keV, 10^{-13} erg cm^{-2} s^{-1})	$4.4^{+0.5}_{-1.4}$	$5.3^{+0.8}_{-4.6}$
L_{TH}^{b} (0.5 – 5 keV, 10^{35} erg s^{-1})	$1.8^{+0.2}_{-0.3}$	$2.2^{+0.3}_{-0.5}$
L_{PL}^{b} (5 – 40 keV, 10^{35} erg s^{-1})	$1.3^{+0.1}_{-0.4}$	$1.6^{+0.2}_{-1.4}$
f_{X}^{a} (0.5 – 60 keV, 10^{-13} erg cm^{-2} s^{-1})	$14.1^{+2.1}_{-4.2}$	$15.4^{+1.7}_{-5.9}$
L_{X}^{b} (0.5 – 60 keV, 10^{35} erg s^{-1})	$5.2^{+1.2}_{-1.6}$	$5.4^{+1.0}_{-3.4}$
$N_{\text{H,LMC}}$ (10^{21} cm^{-2})	3.4 ± 1.0	$2.7^{+0.7}_{-0.6}$
χ^2/ν	305.5/279	299.8/278

NOTE. — Uncertainties are with a 90% C.L. The Galactic column is fixed at $N_{\text{H,Gal}} = 6 \times 10^{20}$ cm^{-2} . $d = 50$ kpc is assumed.

^a The observed flux.

^b The X-ray luminosity after removing the absorption.

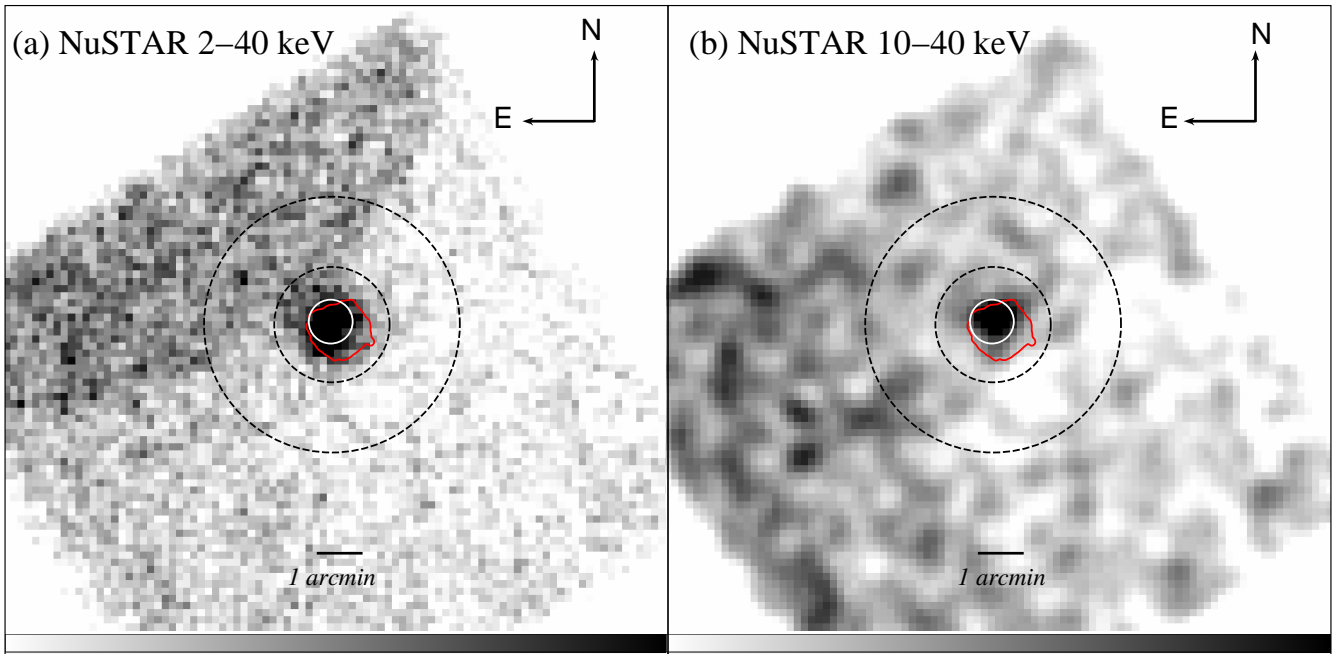


FIG. 1.— (a) Grey-scale *NuSTAR* images of SGR 0526–66: (a) the 2 – 40 keV band, and (b) the 10 – 40 keV band. For the purposes of display both images have been binned by 4×4 pixels. In (b), the image has also been smoothed. In (a) and (b), our source region for 0526–66 is marked with a white circle. The annular background region is marked with dashed circles. The outer boundary of the LMC SNR N49 (taken from the archival *Chandra* ACIS data) is shown with red contours.

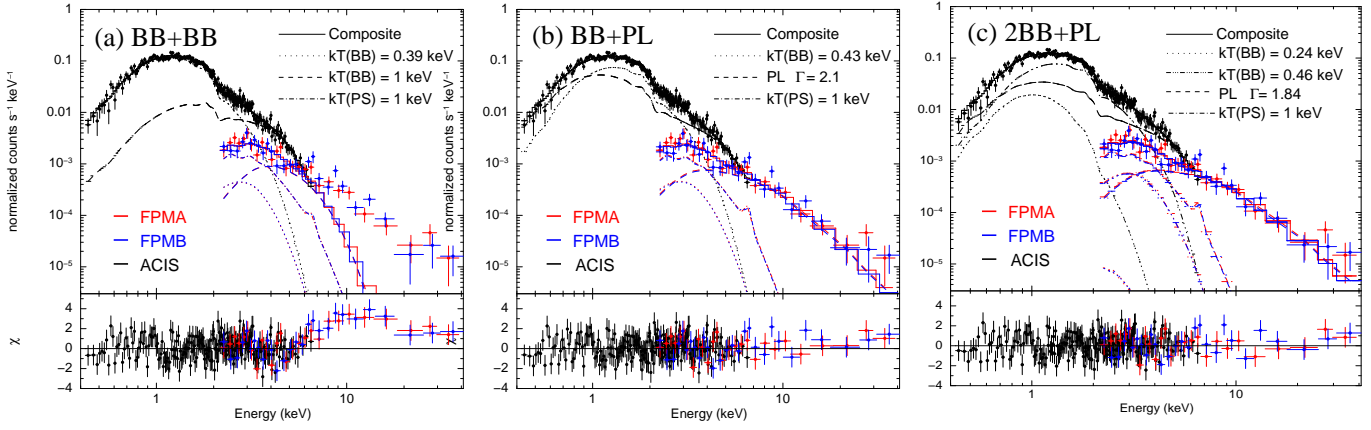


FIG. 2.— The observed *NuSTAR* and *Chandra* spectra of 0526-66. The best-fit models are overlaid in each panel: (a) 2BB, (b) BB+PL, and (c) 2BB+PL. The PS component (with $kT = 1$ keV, representing the contamination by thermal X-ray emission from SNR N49) is shown for the *NuSTAR* spectrum. The lower panels are residuals from the best-fit model.

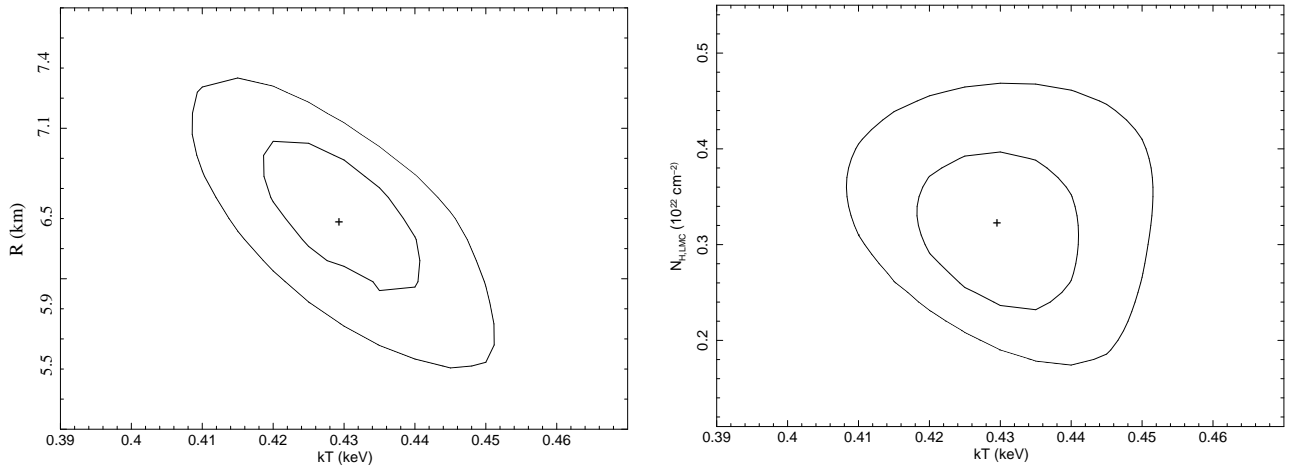


FIG. 3.— (a) The BB temperature vs. emission region radius (at $d = 50$ kpc), and (b) the BB temperature vs. $N_{\text{H,LMC}}$ contour plots based on our best-fit BB + PL model (Table 1). In (a) and (b), 90% and 99% contours are shown. The best-fit temperature and emitting radius are marked with a cross.